

Structure of Rhodopsin in Monolayers at the Air–Water Interface: a PM-IRRAS and X-Ray Reflectivity Study[†]

Hugo Lavoie,[‡] Bernard Desbat,[§] David Vaknin,^{||} and Christian Salesse^{*:‡}

Département de Chimie-Biologie, Université du Québec à Trois-Rivières, Québec, Canada, G9A 5H7, Centre de Recherche en Sciences et Ingénierie des Macromolécules, Université Laval, Ste-Foy, Québec, Canada, G1K 7P4, Laboratoire de Physico-Chimie Moléculaire, URM 5803 Université Bordeaux I, 33405 Talence, France, and Ames Laboratory and Department of Physics, Iowa State University, Ames, Iowa 50011

Received April 23, 2002; Revised Manuscript Received August 27, 2002

ABSTRACT: Monomolecular films of the membrane protein rhodopsin have been investigated in situ at the air–water interface by polarization modulation infrared reflection absorption spectroscopy (PM-IRRAS) and X-ray reflectivity in order to find conditions that retain the protein secondary structure. The spreading of rhodopsin at 0 or 5 mN m⁻¹ followed by a 30 min incubation time at 21 °C resulted in the unfolding of rhodopsin, as evidenced from the large increase of its molecular area, its small monolayer thickness, and the extensive formation of β -sheets at the expense of the α -helices originally present in rhodopsin. In contrast, when spreading is performed at 5 or 10 mN m⁻¹ followed by an immediate compression at, respectively, 4 or 21 °C, the secondary structure of rhodopsin is retained, and the thickness of these films is in good agreement with the size of rhodopsin determined from its crystal structure. The amide I/amide II ratio also allowed to determine that the orientation of rhodopsin only slightly changes with surface pressure and it remains almost unchanged when the film is maintained at 20 mN m⁻¹ for 120 min at 4 °C. In addition, the PM-IRRAS spectra of rod outer segment disk membranes in monolayers suggest that rhodopsin also retained its secondary structure in these films.

Monolayer formation and molecular packing at air–water interfaces is an intriguing issue in the basic research of bio- and artificial membranes, and also in surface science, molecular manipulation, and film patterning. With the advent of surface-sensitive techniques (i.e., synchrotron X-rays, microscopy, FTIR, and others) simple long-chain monomolecular layers at the air–water interfaces have been widely used to shed light on some aspects of biomembrane characteristics (for recent reviews, see refs 1 and 2). To elucidate processes near biomembranes, extensive studies of the interaction between lipid monolayers and soluble proteins in the subphase have been conducted using a variety of methods (for a review, see ref 3). Membrane proteins which are embedded in a lipid bilayer have been purified and spread at air–water interfaces. For example, purified proteins such as rhodopsin (4–9), photosystem II reaction center (10–13), photosystem II core complex (PSII CC) (14, 15), and the serotonin receptor (16, 17) have been studied at the air–water interface. Moreover, liposomes containing membrane

proteins (18, 19) and whole biomembranes such as rod outer segment (ROS) disk membranes (4, 8, 20, 21), purple membranes (22–29), sarcoplasmic reticulum (30, 31), erythrocyte membranes (30, 32), intestinal brush border (32), cytoplasmic membrane of *Escherichia coli* (32), myelin (33), and axolemma membrane (34, 35) have been studied in monolayers at the air–water interface. However, the high surface tension of water can lead to protein unfolding (36) and the structure of these proteins must be assessed prior to drawing conclusions on their properties in these films.

Rhodopsin is a member of the large family of G-protein coupled receptors. It is found in ROS disk membranes, where it constitutes 80% of the total protein content and 95 mol % of membrane proteins (37). It contains seven transmembrane α -helices, and its chromophore, 11-cis retinal, is covalently bound to lysine 296 through a Schiff base linkage (for a review on the structure of rhodopsin, see ref 38). Rhodopsin is covalently modified by the addition of two N-linked oligosaccharides at asparagines 2 and 15 and by palmitoylation at cysteines 322 and 323. An essential disulfide bond has also been identified between cysteines 110 and 187. Its structure has been recently determined at 2.8 Å resolution (38, 39). We have undertaken this study to assess the state of rhodopsin in monolayers at the air–water interface and to search for appropriate conditions that retain protein secondary structure in these films.

In situ techniques to probe monomolecular layers at the air–water interface are well established by now. For instance, X-ray and neutron reflectivity and grazing incidence diffraction of free liquid surfaces allow determination of the

[†] The authors are indebted to the Natural Sciences and Engineering Research Council of Canada for financial support. H.L. also thanks SPPUQTR and FUQTR for a scholarship. CS is a Chercheur-Boursier national of the Fonds de Recherche en Santé du Québec. Ames Laboratory is operated for the U.S. Department of Energy by Iowa State University under Contract No. W-7405-Eng-82. The work at Ames was supported by the Director for Energy Research, Office of Basic Energy Sciences. We are also indebted to NATO for a Collaborative Research grant.

* Corresponding author. Phone: (819) 376-5011 (ext. 3308). Fax: (819) 376-5057. E-mail: christian_salesse@uqtr.ca.

[‡] Université du Québec à Trois-Rivières and Université Laval.

[§] Université Bordeaux I.

^{||} Iowa State University.

electron density across the interface and two-dimensional arrangements in the film on a molecular length scale (40). Infrared reflection absorption spectroscopy (IRRAS) (41) and polarization modulation infrared reflection absorption spectroscopy (PM-IRRAS) (42) are additional powerful tools that were recently used to extract information on the secondary structure and orientation of peptide and protein monolayers at the air–water interface (14, 43–51). In the present study, X-ray reflectivity and PM-IRRAS were combined to carefully investigate the structure of Langmuir monolayers of the purified membrane protein rhodopsin in detergent as well as in its lipid environment of ROS disk membranes. We demonstrate the effect of different parameters on rhodopsin structure in situ at the air–water interface.

EXPERIMENTAL PROCEDURES

Purification of Rod Outer Segment Disk Membranes and Rhodopsin. All manipulations involving rhodopsin were carried under dim red light ($\lambda > 650$ nm). Highly purified bovine ROS membranes were prepared by continuous sucrose concentration gradient as previously described (52). Purification of ROS disk membranes was then achieved by flotation on Ficoll as described previously (53) with slight modifications (54). ROS were solubilized in ammonyx LO, and rhodopsin was purified by concanavalin A-sepharose 4B affinity chromatography and the detergent was changed for octyl glucoside as described by Litman (55) and modified by Salesse et al. (4). An absorbance ratio ($A_{280\text{ nm}}/A_{500\text{ nm}}$) of 1.8 was obtained for the purity of rhodopsin which is comparable to published data (55). The concentration of the rhodopsin samples was determined by absorption spectroscopy using an extinction coefficient of $40\,000\text{ L mol}^{-1}\text{ cm}^{-1}$ at 500 nm. The buffer used to prepare the solution of rhodopsin for monolayer measurements contained 10 mM phosphate buffer (pH 7.2) and 30 mM octyl glucoside. The same buffer without octyl glucoside was used to spread ROS disk membranes.

Film Formation. The water used to prepare the monolayer subphase was purified by filtration on Millipore (18.2 MOhm cm). Rhodopsin and ROS disk membranes were spread onto a subphase containing 10 mM phosphate buffer (pH 7.2) and 100 mM NaCl using the method of Trurnit (56) as described earlier in detail (4). The method of Trurnit allows quantitative spreading of proteins. The presence of NaCl is essential for the formation of monolayers of membrane proteins (30). In fact, in the absence of NaCl, no isotherm can be measured unless a very large amount of protein is spread. A volume of 50, 100, or 200 μL from a 1.5×10^{-5} M rhodopsin solution was spread in monolayer to reach a surface pressure of 0, 5, or 10 mN m^{-1} , respectively. The surface of the trough was 919.6 cm^2 . A molecular weight of 42 000 Da for rhodopsin was used in estimating its area per molecule. Surface pressure–area isotherms were measured using a homemade Langmuir trough with a Wilhelmy type balance which has been described elsewhere (15). The possible loss of rhodopsin in the subphase upon spreading was previously ruled out by the demonstration that the molecular area of rhodopsin remained unchanged after 10 agitations of the subphases and that the surface pressure isotherms of rhodopsin are highly reproducible (4).

PM-IRRAS Measurements. PM-IRRAS spectra were recorded at the air–water interface by co-addition of 800 scans

at a resolution of 8 cm^{-1} using a Nicolet 740 spectrometer following an experimental procedure previously described (42). The PM-IRRAS spectra of covered surface, S_{film} , as well as that of the bare water, S_{w} , were measured, and the normalized difference $\Delta S = [S_{\text{film}} - S_{\text{w}}]/S_{\text{w}}$ is presented. On dielectric substrates, PM-IRRAS presents a specific surface selection rule, such that a transition moment lying in the plane or perpendicular to the surface yields a positive or a negative absorption band, respectively (57). For an intermediate orientation of the transition moment, the two contributions are competing, and the absorption band vanishes when the transition moment is tilted at approximately 39° from the surface normal to the water subphase (57).

X-Ray Reflectivity. X-ray reflectivity measurements were performed in situ at the air–water interface on a liquid surface reflectometer at Ames Laboratory. This reflectometer has been described elsewhere in details (58). In short, an X-ray beam of wavelength $\lambda = 1.5404\text{ \AA}$ was selected by Bragg reflection from the (111) planes of a single crystal Ge monochromator. The intensity of the incident beam was continuously monitored to account for possible fluctuations of the X-ray beam. To reduce surface waves during measurements, a glass plate was positioned in the trough under the X-ray beam footprint. The subphase depth above the glass plate was kept at approximately 0.3 mm thick. A dynamic vibration isolation system (JRS MOD-2 Affoltern, Switzerland) was used to eliminate mechanical vibrations. The Langmuir trough was contained in an airtight aluminum enclosure with Kapton windows, and its temperature was constantly maintained at 20°C . The sealed container was flushed with helium for 1 h before the beginning of the X-ray measurements to reduce background due to air scattering. Gas flow was allowed during compression of the monolayer to the required surface pressure, and it was stopped during X-ray data collections.

The specular X-ray experiments yield the electron density profiles across the interface and can be related to molecular arrangements in the film. The electron density profile across the interface $r(z)$ is extracted by refining the multiple slab model that best fits the measured reflectivity using a nonlinear least-squares method. The reflectivity from the slab model at a momentum transfer Q_z is calculated by (40, 59)

$$R(Q_z) = R_0(Q_z)e^{(Q_z\sigma)^2} \quad (1)$$

where $R_0(Q_z)$ is the reflectivity from steplike functions calculated by the recursive dynamical method (60), and σ is an effective surface roughness, accounting for the smearing of all interfaces (conformal surface roughness) due to thermal capillary waves and surface inhomogeneities (40, 61).

Surface Roughness. The surface roughness of a pure liquid–vapor interface is dominated by thermally excited capillary waves, σ_{CW} , that depend on surface tension γ ($\sigma_{\text{CW}}^2 \propto k_B(T/\gamma)$). In addition, the effective surface roughness σ depends on the intrinsic roughness σ_i , due to the size, shape and organization of the molecule at the interface. Therefore, the measured effective roughness from the reflectivity is given by (61)

$$\sigma^2 = \sigma_{\text{CW}}^2 + \sigma_i^2 \quad (2)$$

For pure liquids, in particular for water, the intrinsic part is

comparable or smaller than the capillarity waves term. Under the vibration damping conditions described above (glass plate and dynamic anti-vibration system), the effective surface roughness from pure water (or subphase) is approximately 2.4–2.8 Å, depending on the resolution of the spectrometer and the attenuation of waves at the interface. For typical Langmuir monolayers (i.e., fatty acids, lipids, etc.), there is a small increase in the surface roughness, which is usually associated with the increase of surface pressure (or equivalently the decrease of surface tension) as discussed above (40). The effective surface roughness for these monolayers at moderate surface pressure (20–35 mN m⁻¹) is in the range 2.8–4.0 Å.

RESULTS

Protein properties can be drastically altered when spread in monolayers at the air–water interface (36, 62). We have previously demonstrated that the initial surface pressure of spreading and the incubation of PSII CC at low surface pressure were very critical parameters for its structure in monolayers (14, 15). Lowering the temperature was shown to reduce protein unfolding whereas compression speed had no effect on the structure of PSII CC (14). These parameters were thus also used to find the most appropriate experimental conditions to retain the properties of rhodopsin in monolayers at the air–buffer interface.

Effect of Temperature and Spreading Surface Pressure on the Molecular Area of Rhodopsin. Very similar isotherms of rhodopsin are measured at 4 and 21 °C (curves a and b, respectively, Figure 1A) when the film is spread at an initial surface pressure of 0 mN m⁻¹, incubated for 30 min, and then compressed at a speed of 1 nm² molecule⁻¹ min⁻¹. In fact, only a small difference in collapse pressure and in molecular area can be observed between these two isotherms. For both temperatures, surface pressure rise begins at ~61 nm² molecule⁻¹, and the collapse of the monolayer at 21 °C occurs at 43.8 mN m⁻¹ (15.8 nm² molecule⁻¹) compared to 42 mN m⁻¹ (14 nm² molecule⁻¹) at 4 °C. The isotherms shown in Figure 1A are slightly shifted to lower molecular areas by ~0.4 nm² molecule⁻¹ compared the one reported by Salesse et al. (4). This difference can be explained by the fact that, in their experiments (4), the rhodopsin monolayer was incubated at 0 mN m⁻¹ for a period of time much longer than the 30 min incubation time in the present study. Such a long incubation at low surface pressure could explain their slightly larger molecular area if more extensive unfolding of rhodopsin had taken place.

In contrast, very different isotherms are measured at 4 and 21 °C when the film is spread at an initial surface pressure of 5 mN m⁻¹ and then immediately compressed at a speed of 4.5 nm² molecule⁻¹ min⁻¹ (Figure 1B). Indeed, the isotherm at 4 °C (curve a, Figure 1B) is found at a much lower molecular area than that at 21 °C (curve b, Figure 1B). Moreover, no collapse can be distinguished in the isotherm at 4 °C up to 48 mN m⁻¹, whereas a clear collapse can be seen at 42 mN m⁻¹ in the isotherm at 21 °C. The most striking feature is that both isotherms of Figure 1B are shifted to lower molecular areas compared to those shown in Figure 1A. These data suggest that rhodopsin is unfolded when spreading is performed at 21 °C (Figure 1A) whereas unfolding is prevented when the film is spread at an initial

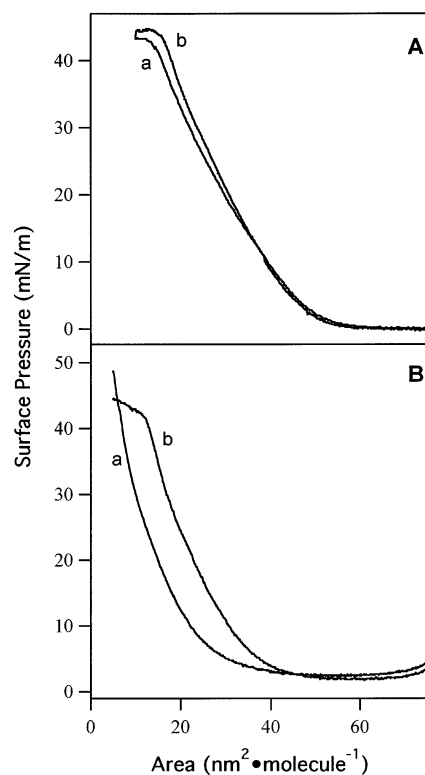


FIGURE 1: Surface pressure isotherms of pure rhodopsin at the air–water interface on a subphase buffer containing 10 mM phosphate buffer (pH 7.2) and 100 mM NaCl. (A) Spreading at 0 mN m⁻¹ followed by a 30 min incubation time; compression speed is 1 nm² molecule⁻¹ min⁻¹; subphase temperature is 4 (curve a) and 21 °C (curve b). (B) Spreading at 5 mN m⁻¹ followed by an immediate compression; compression speed is 4.5 nm² molecule⁻¹ min⁻¹; subphase temperature is 4 (curve a) and 21 °C (curve b).

surface pressure of 5 mN m⁻¹ at 4 °C followed by an immediate compression (curve a, Figure 1B).

Infrared Spectrum of Rhodopsin in ROS Disk Membranes. Since spreading of pure rhodopsin in monolayers at the air–buffer interface could lead to protein unfolding, the infrared spectrum of ROS disk membranes was measured in solution in order to get the spectrum of rhodopsin in its native environment. This spectrum will thus provide information on the shape and position of the bands of rhodopsin. Rhodopsin is by far the main component of ROS disk membranes, as it comprises 95 mol % of membrane proteins (37). The spectrum in Figure 2 from 1400 to 1800 cm⁻¹ shows that the amide I and the amide II vibrations of the protein backbone are centered at 1655 and 1545 cm⁻¹, respectively. The position of these bands is in very good agreement with the data reported on rhodopsin (63, 64). Given that there are 72 lipids per rhodopsin in ROS disk membranes (65), a lipid ester carbonyl stretch vibration can be identified at 1734 cm⁻¹, which is in very good agreement with other reports (63, 64). Previous studies have shown that a direct correlation exists between the frequency of the amide I band and protein secondary structure (66, 67). The position of the amide I band at 1655 cm⁻¹ suggests that rhodopsin contains an extensive proportion of α -helices as clearly demonstrated in the high-resolution structure of rhodopsin (38, 39). Indeed, rhodopsin contains 7 transmembrane α -helices as well as a smaller α -helix located in the C-terminal region which is parallel to the plane of the membrane. In addition, the position of the shoulder at 1632

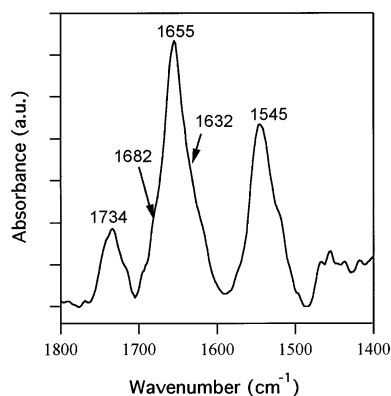


FIGURE 2: FTIR buffer subtracted spectrum of rod outer segment disk membranes in 10 mM phosphate buffer (pH 7.2) and 100 mM NaCl from 1400 to 1800 cm^{-1} at room temperature between two CaF_2 windows (the path length is 5 μm) with a spectral resolution of 4 cm^{-1} . Spectrum was obtained with 300 scans for both the sample and the reference using a Nicolet 850.

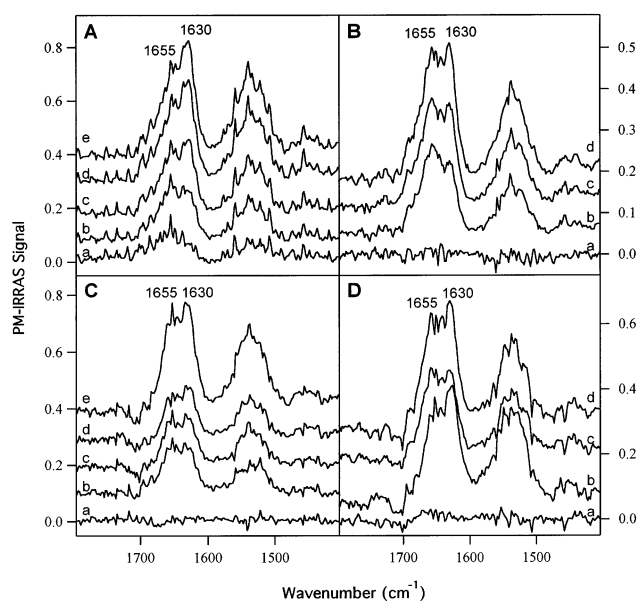


FIGURE 3: PM-IRRAS spectra of pure rhodopsin in monolayers at different surface pressures. (A and B) Spreading at 0 mN m^{-1} followed by a 30 min incubation time. (C and D) Spreading at 5 mN m^{-1} followed by a 30 min incubation time. Compression speed is 1 (A and C) and 4.5 $\text{nm}^2 \text{molecule}^{-1} \text{min}^{-1}$ (B and D). Spectra a to e were measured at 0, 10, 20, 30, and 40 mN m^{-1} , respectively (A and C). Spectra a to d were measured at 0, 10, 20, and 30 mN m^{-1} , respectively (B and D). Subphase temperature is 21 $^\circ\text{C}$. The spreading surface pressure of 5 mN m^{-1} (C and D) decreases to 0 mN m^{-1} during the 30 min incubation time, which allows the measurement of a first spectrum at 0 mN m^{-1} .

cm^{-1} and the weaker vibration near 1685 cm^{-1} in the spectrum indicate the presence of a certain amount of β -sheet conformation in rhodopsin (68–70). In fact, the high-resolution structure of rhodopsin clearly shows the presence of one antiparallel β -sheet in the loop between α -helices 4 and 5 and another one near the N-terminal (38, 39). Moreover, this spectrum presents an amide I/amide II ratio of 1.47 which is very similar to the data obtained by other groups (63, 64).

Effect of Different Parameters on the Structure of Rhodopsin in Monolayers. Figure 3 presents the PM-IRRAS spectra of pure rhodopsin at 21 $^\circ\text{C}$ at different surface pressures at the air–buffer interface. These spectra were measured after

spreading rhodopsin at an initial surface pressure of 0 mN m^{-1} followed by a 30 min incubation time prior to compression (Figure 3A,B) or at an initial surface pressure of 5 mN m^{-1} followed by a 30 min incubation time prior to compression (Figure 3C,D). The compression speed for the spectra shown in Figure 3A,C was 1 $\text{nm}^2 \text{molecule}^{-1} \text{min}^{-1}$ compared to 4.5 $\text{nm}^2 \text{molecule}^{-1} \text{min}^{-1}$ for those presented in Figure 3B,D. When compared to the spectrum of rhodopsin in ROS disk membranes shown in Figure 2, all of these spectra show clear signs of protein unfolding. Indeed, two components in the amide I band at 1655 and 1630 cm^{-1} with varying intensities can be seen in these spectra, which indicate the presence of both α -helices and β -sheets. Therefore, these experimental conditions lead to the formation of additional β -sheets at the expense of the α -helices originally present in rhodopsin (compare Figures 2 and 3). The effect of compression rate can be readily seen when comparing Figure 3A,B. Indeed, the ratio between the components of the amide I band at 1630 and 1655 cm^{-1} in the spectra of Figure 3A,B suggests that more β -sheets are formed when the rhodopsin film is compressed at a speed of 1 $\text{nm}^2 \text{molecule}^{-1} \text{min}^{-1}$ than at 4.5 $\text{nm}^2 \text{molecule}^{-1} \text{min}^{-1}$. However, orientational changes can be responsible for part of the decrease of the intensity of the amide I observed in Figure 3. Indeed, if the α -helices become oriented more perpendicular to the normal to the interface when unfolding takes place, the intensity of the amide I will decrease (43). However, in our experiments, the most important indication of unfolding is the observation of a shoulder at the position which is typical for β -sheets (1630 cm^{-1}). In addition, it is known that very strong intermolecular interactions between protein molecules in solution can result in the observation of a band for aggregated proteins below 1620 cm^{-1} . The possible contribution of aggregated rhodopsin to the band at 1630 cm^{-1} in the spectra of Figure 3 cannot be ruled out. This is, however, rather unlikely because there is no sign for the presence of a band at this position at molecular areas of rhodopsin which should promote protein aggregation because rhodopsin surface concentration is very high and a large share of the detergent is solubilized in the subphase (see Figures 6 and 8 below). Nevertheless, altogether these data suggest that spreading rhodopsin at 0 mN m^{-1} followed by a 30 min incubation time at a compression speed of 1 $\text{nm}^2 \text{molecule}^{-1} \text{min}^{-1}$ (Figure 3A) are the most harmful experimental conditions for rhodopsin. The thickness of the rhodopsin film under these conditions was then measured by X-ray reflectivity.

Figure 4A shows an X-ray reflectivity curve normalized to the reflectivity of an ideally flat subphase (R/R_F) versus the momentum transfer (Q_z) of the rhodopsin monolayer spread at an initial surface pressure of 0.1 mN m^{-1} . The solid line in Figure 4A is the best-fit calculated reflectivity from the electron density model structure shown in Figure 4B as a solid line. The reflectivity was calculated by assuming a two-box model (40). The dotted line in Figure 4B corresponds to the box model in the absence of the effect of surface roughness. The thickness values of the two boxes extracted from the reflectivity are 22.9 ± 2 and 17.6 ± 2 \AA with electron number densities of 0.35 ± 0.02 and 0.39 ± 0.02 $\text{e}/\text{\AA}^3$, respectively, and a surface roughness $\sigma = 3.2 \pm 0.5$ \AA . The two-box model suggests that rhodopsin may be composed of two distinct electron density zones. The total

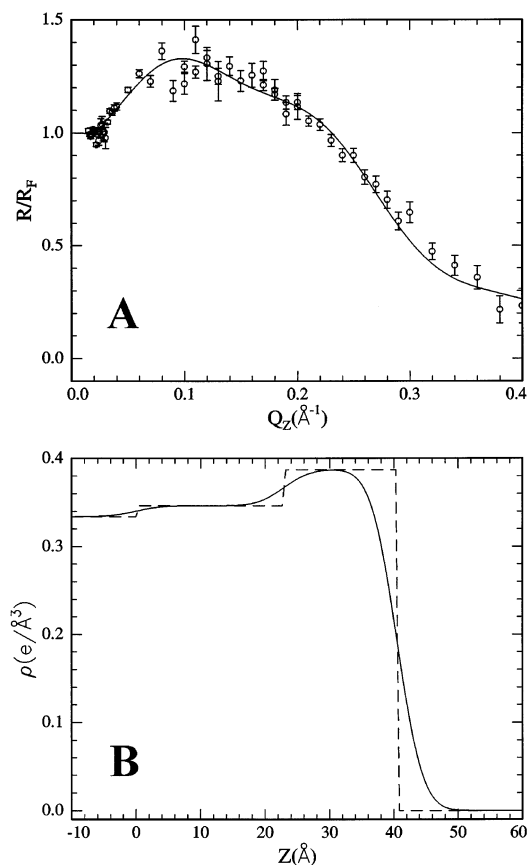


FIGURE 4: (A) X-ray reflectivity (normalized to the Fresnel reflectivity R_F of ideally flat subphase) vs momentum transfer Q_z of a rhodopsin monolayer at 0.1 mN m^{-1} . The solid line is the calculated reflectivity obtained from the scattering length density profile shown as a solid line in (B). The dotted line in panel B corresponds to the box model that is smeared by a Gaussian to give the solid curve. Subphase temperature is 20°C .

thickness of the rhodopsin film as extracted from the box model in the absence of surface roughness is $40.5 \pm 4 \text{ \AA}$. This thickness value is much smaller than the size of rhodopsin (75 \AA) determined directly from its crystal structure (38, 39) and thus suggests that rhodopsin is unfolded under these conditions. Given that low surface pressure and incubation time result in rhodopsin unfolding, the effect of spreading at 5 mN m^{-1} and of an immediate compression after spreading on the structure of rhodopsin was then investigated by PM-IRRAS.

Figure 5 presents the PM-IRRAS spectra measured at 21°C after spreading rhodopsin at an initial surface pressure of 5 mN m^{-1} followed by an immediate compression at a speed of 1 (Figure 5A) or 4.5 (Figure 5B) $\text{nm}^2 \text{ molecule}^{-1} \text{ min}^{-1}$. This initial surface pressure of 5 mN m^{-1} quickly decreases to 0 (Figure 5A) and $\sim 2 \text{ mN m}^{-1}$ (Figure 5B) and then remains constant until the onset of the surface pressure rise at the beginning of the isotherm of rhodopsin. It can be seen that the increase of compression speed by a factor of 4.5 (or an equivalent decrease in compression time) highly improved the quality of the spectra of rhodopsin when compared to the spectrum of rhodopsin in ROS disk membranes (Figure 2). Indeed, a faster compression speed allows to retain a larger proportion of the α -helices of rhodopsin (compare Figure 5A,B). Only a shoulder at 1630 cm^{-1} is observed in these spectra (Figure 5B) in contrast to

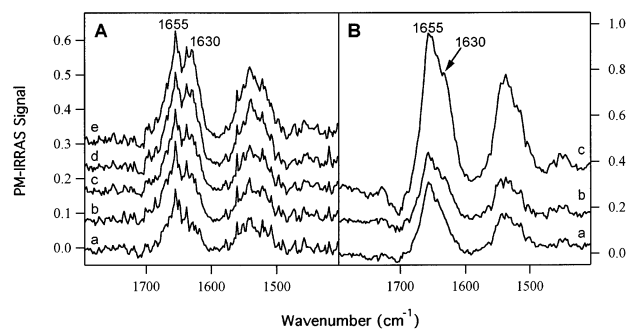


FIGURE 5: PM-IRRAS spectra of pure rhodopsin in monolayers at different surface pressures. (A) Spreading at 5 mN m^{-1} followed by an immediate compression at a speed of $1 \text{ nm}^2 \text{ molecule}^{-1} \text{ min}^{-1}$. Spectra a–e were measured, respectively, at $0, 10, 20, 30,$ and 40 mN m^{-1} . (B) Spreading at 5 mN m^{-1} followed by an immediate compression at a speed of $4.5 \text{ nm}^2 \text{ molecule}^{-1} \text{ min}^{-1}$. Spectra a–c were measured at, respectively, $10, 20,$ and 30 mN m^{-1} . Subphase temperature is 21°C . The spreading surface pressure of 5 mN m^{-1} decreases to 0 mN m^{-1} during the compression at $1 \text{ nm}^2 \text{ molecule}^{-1} \text{ min}^{-1}$ (A), which allows the measurement of a first spectrum at 0 mN m^{-1} .

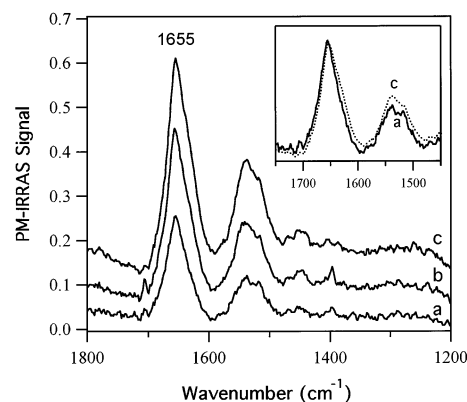


FIGURE 6: PM-IRRAS spectra of pure rhodopsin in monolayers at different surface pressures. Spreading at 10 mN m^{-1} followed by an immediate compression at a speed of $4.5 \text{ nm}^2 \text{ molecule}^{-1} \text{ min}^{-1}$. Spectra a–c were measured, respectively, at $10, 20,$ and 30 mN m^{-1} . In the inset, the spectra at 10 (a, solid line) and 30 (c, dotted line) mN m^{-1} were normalized using the amide I band. Subphase temperature is 21°C .

the strong component at 1630 cm^{-1} in the spectra shown in Figure 5A. However, the intensity of the shoulder in the spectra of Figure 5B, when compared to the shoulder in the spectrum of Figure 2, suggests that rhodopsin is partly unfolded under these conditions. The effect of compression speed suggests that time is a critical parameter in the unfolding of rhodopsin in monolayers. In addition, the decrease in surface pressure observed immediately after spreading could contribute to the unfolding of rhodopsin.

To evaluate the effect of the decrease in surface pressure during compression prior to the onset of the surface pressure rise, PM-IRRAS spectra of rhodopsin were measured at 21°C after spreading at an initial surface pressure of 10 mN m^{-1} followed by an immediate compression at a speed of $4.5 \text{ nm}^2 \text{ molecule}^{-1} \text{ min}^{-1}$ (see Figure 6). This initial surface pressure of spreading quickly decreased down to $\sim 4.5 \text{ mN m}^{-1}$ during compression, and this surface pressure remained constant during the rest of the compression until the onset of the surface pressure rise. It can be seen in Figure 6 that the amide I band in these spectra is centered at 1655 cm^{-1} and that there is no sign of rhodopsin unfolding. Indeed, the

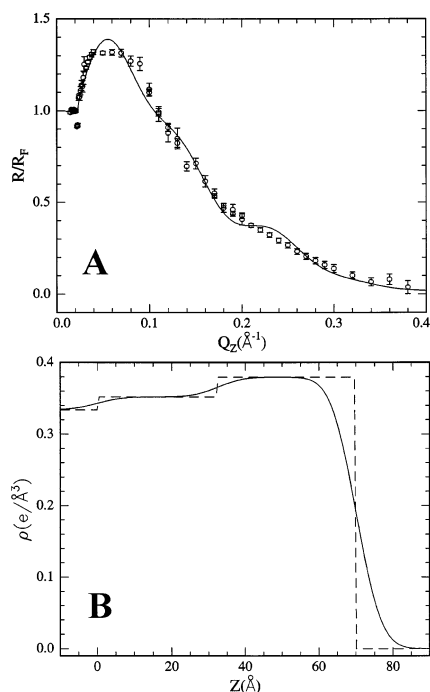


FIGURE 7: (A) X-ray reflectivity (normalized to the Fresnel reflectivity R_F of ideally flat subphase) vs momentum transfer Q_z of a rhodopsin monolayer at 11.7 mN m^{-1} . The solid line is the calculated reflectivity obtained from the scattering length density profile shown as a solid line in panel B. The dotted line in panel B corresponds to the box model that is smeared by a Gaussian to give the solid curve. Subphase temperature is 20°C .

presence of a shoulder at 1630 cm^{-1} can hardly be distinguished in these spectra, whereas it was obvious in the spectra shown in Figure 5B. It can thus be postulated that when a surface pressure of at least 4.5 mN m^{-1} is maintained during compression at 21°C , no unfolding occurs in the rhodopsin film. Such a surface pressure might be sufficient to provide lateral interactions between rhodopsin molecules and thus prevent its unfolding. The thickness of the rhodopsin film under these conditions was then measured by X-ray reflectivity.

Figure 7A shows an X-ray reflectivity curve normalized to the reflectivity of an ideally flat subphase (R/R_F) versus the momentum transfer (Q_z) of the rhodopsin monolayer spread at an initial surface pressure of 9.5 mN m^{-1} . The dotted line in Figure 7B corresponds to the box model in the absence of the effect of surface roughness. The thickness values of the two boxes extracted from the reflectivity are $30 \pm 2 \text{ \AA}$ and $37.5 \pm 2 \text{ \AA}$ with electron number densities of 0.35 ± 0.02 and $0.38 \pm 0.02 \text{ e/\AA}^3$, respectively, and a surface roughness $\sigma = 5.4 \pm 0.5 \text{ \AA}$. The two-box model suggests that rhodopsin may be composed of two distinct electron density zones. The roughness is too large to be accounted for by capillary waves only, and possibly the roughness is dominated by the intrinsic part, which, using eq 2, is estimated at $\sigma_1 \sim 4.5\text{--}5.0 \text{ \AA}$. The total homogeneous thickness of the rhodopsin film as extracted from the box model in the absence of surface roughness is $67.5 \pm 4 \text{ \AA}$. This thickness value reflects the average size of the densely packed rhodopsin. The difference between this value of 67.5 \AA and the dimension of rhodopsin perpendicular to the membrane (75 \AA) determined from its crystal structure (38) may be explained by (1) the larger intrinsic roughness of

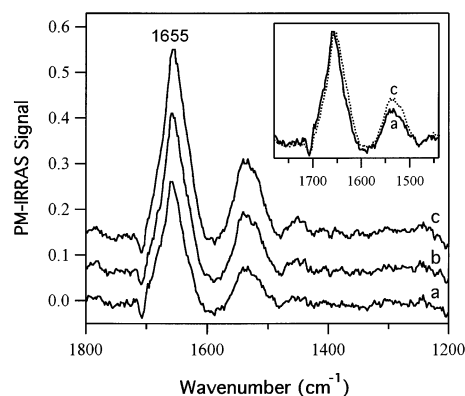


FIGURE 8: PM-IRRAS spectra of pure rhodopsin in monolayers at different surface pressures. Spreading at 5 mN m^{-1} followed by an immediate compression at a speed of $4.5 \text{ nm}^2 \text{ molecule}^{-1} \text{ min}^{-1}$ on a subphase at 4°C . Spectra a–c were measured, respectively, at 10, 20, and 30 mN m^{-1} . In the inset, the spectra at 10 (a, solid line) and 30 (c, dotted line) mN m^{-1} were normalized using the amide I band.

the rhodopsin film which can be associated with the staggering between proteins and with the irregularity inherent to the morphology of rhodopsin, i.e., the presence of the hydrophilic loops that link together the transmembrane α -helices of rhodopsin that are not folded into the densely folded part of the protein, and (2) the fact that the cytoplasmic loops are poorly determined in the model of Teller et al. (38). Nevertheless, these data thus suggest that the dimension of rhodopsin under these experimental conditions is in good agreement with the dimension of crystalline rhodopsin and thus further support our PM-IRRAS evidence that the structure of rhodopsin is retained under these conditions. These data also indicate that the rhodopsin film is composed of a single layer of protein homogeneously distributed at the interface. Since temperature was shown to reduce PSII CC unfolding (14), the effect of lowering the temperature of the subphase on the structure of rhodopsin in monolayers was also studied by PM-IRRAS.

Figure 8 shows the PM-IRRAS spectra of rhodopsin spread at an initial surface pressure of 5 mN m^{-1} at 4°C and compressed immediately at a speed of $4.5 \text{ nm}^2 \text{ molecule}^{-1} \text{ min}^{-1}$. It can be seen that the amide I band is centered at 1655 cm^{-1} and that there is no sign of protein unfolding. It is interesting to compare these data with those presented in Figure 5B because the temperature of the measurement is the only different experimental condition between these two sets of data. The presence of the shoulder at 1630 cm^{-1} is very obvious in the spectra of Figure 5B, whereas there is no obvious sign for the presence of this shoulder in the spectra of Figure 8. It can thus be concluded that lowering the temperature to 4°C prevents rhodopsin unfolding. The stability of rhodopsin structure in monolayers as a function of time was then investigated by PM-IRRAS.

Figure 9 shows the PM-IRRAS spectra measured after spreading rhodopsin at an initial surface pressure of 5 mN m^{-1} followed by an immediate compression at a speed of $4.5 \text{ nm}^2 \text{ molecule}^{-1} \text{ min}^{-1}$ at 4°C until a surface pressure of 20 mN m^{-1} was reached. The spectra were then taken every 30 min for 2 h. It can be seen that the intensity of the amide I band increases during the first 30 min and then remains unchanged (see inset of Figure 9). The inset of this figure also shows normalized spectra at 0 and 120 min

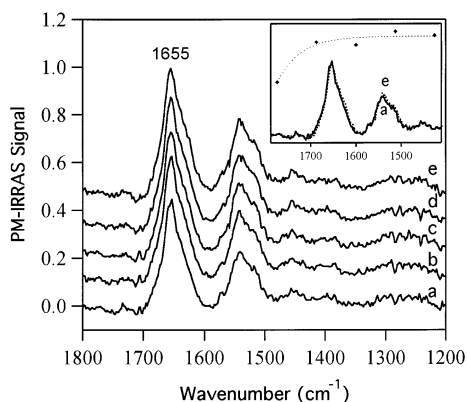


FIGURE 9: PM-IRRAS spectra of pure rhodopsin measured as a function of time. Spreading at 5 mN m^{-1} followed by an immediate compression at a speed of $4.5 \text{ nm}^2 \text{ molecule}^{-1} \text{ min}^{-1}$ on a subphase at 4°C until a surface pressure of 20 mN m^{-1} is reached. Spectra a–e were measured, respectively, at 0, 30, 60, 90, and 120 min. Inset: the upper curve is the plot of the intensity of amide I band as a function of time; the lower curves are the spectra at 0 (a, solid line) and 120 (e, dotted line) min which were normalized using the amide I band.

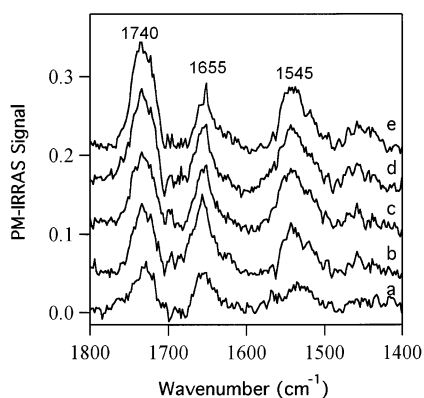


FIGURE 10: PM-IRRAS spectra of ROS disk membranes at different surface pressures. Spectra a–e were measured, respectively, at 0, 10, 20, 30, and 40 mN m^{-1} on a subphase at 21°C . Compression speed is $10 \text{ cm}^2 \text{ min}^{-1}$.

incubation time. The shape of these two spectra is almost identical, which suggests that the secondary structure of rhodopsin remains unchanged when incubated for 120 min at 4°C . Moreover, the fact that the AI/AII ratio remains unchanged (see inset of Figure 9) strongly suggests that the orientation of the α -helices of rhodopsin do not change as a function of time at a surface pressure of 20 mN m^{-1} even though an increase of the intensity of the amide I band is observed during the first 30 min of incubation.

PM-IRRAS Spectra of Monolayers of ROS Disk Membranes. Figure 10 shows the PM-IRRAS spectra of a film of ROS disk membranes spread at the air–buffer interface at an initial surface pressure of 0, 5, or 10 mN m^{-1} without any noticeable change in the shape of the amide I band. These spectra show a band at 1740 cm^{-1} attributed to the ester carbonyl ($\nu_s \text{ C=O}$) of the membrane phospholipids, an amide I band centered at 1655 cm^{-1} , and the amide II vibration band at 1545 cm^{-1} . It can also be seen that the intensity of the amide I band of pure rhodopsin monolayers is approximately twice as large as that of ROS disk membranes at the same surface pressure (compare Figures 6 and 8 with Figure 10). Although water vapor bands are not very well compensated in the spectra shown in Figure 10, the position

of the amide I band is centered at approximately 1655 cm^{-1} , and there is no obvious sign of unfolding whatever spreading is performed at 0 mN m^{-1} or at higher values of initial surface pressure.

DISCUSSION

The combination of the measurement of surface pressure isotherms with X-ray reflectivity and PM-IRRAS provides a significant contribution to the improvement of our knowledge of the structural properties of membrane proteins spread in monolayers at the air–water interface. Indeed, molecular information on the secondary structure of rhodopsin has been obtained together with film thickness, which allowed a thorough characterization of the behavior of rhodopsin in monolayers. The results demonstrated that the surface pressure of spreading, the compression speed, the surface pressure prior to the onset of the isotherm, and the temperature are very important parameters to retain the α -helical secondary structure of rhodopsin in monolayers. In contrast, the experimental conditions widely used to form films of amphiphilic molecules at the air–water interface (initial low surface pressure prior to compression, incubation of the film at zero surface pressure to allow solvent evaporation as well as low rate of compression) when applied to rhodopsin lead to the alteration of its secondary structure.

Low Surface Pressure and Incubation Time Result in Rhodopsin Unfolding in Monolayers. A positive surface pressure of $2\text{--}3 \text{ mN m}^{-1}$ is routinely obtained after spreading rhodopsin, regardless of the amount of protein spread. This surface pressure decreases to 0 mN m^{-1} during the 30 min incubation time (Figure 1A), most likely because of the loss of octyl glucoside in the subphase, and results in rhodopsin unfolding (Figure 3A,B). At this point, the molecular area available for rhodopsin is very large ($77 \text{ nm}^2 \text{ molecule}^{-1}$), and unfolding cannot be prevented, as shown in Figure 3A,B. Protein unfolding leads to a large increase of molecular area as we have previously demonstrated for PSII CC (15). Indeed, spreading of PSII CC at an initial surface pressure of 0 mN m^{-1} followed by a 30 min incubation time leads to a molecular area twice as large as that when spreading was performed at an initial surface pressure of 5.7 mN m^{-1} followed by an immediate compression (15). This increase in molecular area was clearly shown to result from the unfolding of PSII CC (14, 15). Similar results are obtained with rhodopsin. Indeed, both isotherms of Figure 1A are shifted to larger molecular areas compared to those shown in Figure 1B because rhodopsin is unfolded when spreading and incubation is performed at low surface pressure (Figure 1A) whereas unfolding is prevented when the film is spread at an initial surface pressure of 5 mN m^{-1} at 4°C followed by an immediate compression (curve a, Figure 1B). These results thus clearly show that low surface pressure of spreading and incubation of the film prior to compression leads to rhodopsin unfolding. The small thickness value measured for rhodopsin under these conditions also supports this conclusion (Figure 4).

Loss of Octyl Glucoside in the Subphase Is Responsible for Rhodopsin Unfolding. We have previously shown that unfolding of PSII CC was prevented when spreading was performed at 5.7 mN m^{-1} followed by an immediate compression (14). In contrast, unfolding of rhodopsin was

observed under these conditions (Figure 5A,B). The main difference between these two sets of experiments is that no decrease of the spreading surface pressure of 5.7 mN m^{-1} was observed during compression of PSII CC (14, 15) whereas a decrease in surface pressure from 5 to $\sim 2 \text{ mN m}^{-1}$ was observed during compression of the rhodopsin film (Figures 1B and 5B). This behavior can be attributed to the difference in solubility between the detergents dodecyl maltoside and octyl glucoside, which are used to solubilize PSII CC and rhodopsin, respectively. Indeed, no surface pressure was measured after spreading and compression of octyl glucoside alone, the surface pressure being constantly at 0 mN m^{-1} (at both compression speeds), which shows that this detergent is a poor tensioactive molecule (4). In contrast, isotherms of dodecyl maltoside could be measured, and the excess of this detergent was lost in the subphase only at high surface pressure, as clearly demonstrated by the large decrease of the C=O stretching band of dodecyl maltoside at 30 mN m^{-1} when compared to the spectrum at 10 mN m^{-1} (see Figure 4 in ref 14).

Several additional observations suggest that most of the octyl glucoside is lost in the subphase upon spreading and compression of the rhodopsin film, which results in protein unfolding. Indeed, the initial surface pressure of spreading of 5 mN m^{-1} (Figure 3C,D) decreases to almost 0 mN m^{-1} during the 30 min incubation time. In addition, when the rhodopsin film is immediately compressed at a low rate of compression ($1 \text{ nm}^2 \text{ molecule}^{-1} \text{ min}^{-1}$, Figure 5A), the initial surface pressure of 5 mN m^{-1} decreases to 0 mN m^{-1} prior to the onset of the surface pressure rise. Given that there is a large excess of the number of octyl glucoside molecules over the number of rhodopsin molecules (~ 2500) in the spreading solution and that octyl glucoside is a poor tensioactive molecule, it was postulated that the octyl glucoside molecules which are not involved in close interactions with rhodopsin are lost in the subphase (4). This is further evidenced by the data presented in Figure 9. Indeed, when compression is stopped at 20 mN m^{-1} , the slow decrease in surface pressure is compensated by compression of the film, which leads to an increase of the intensity of the amide I band during the first 30 min of incubation of the film and thus to an increase in rhodopsin concentration per unit of surface (see inset of Figure 9). Given that rhodopsin quantitatively remains at the surface upon spreading (4) and that octyl glucoside is the only component present in the spreading solution in addition to rhodopsin, the observation of a decrease in surface pressure combined with an increase in the intensity of the amide I band of rhodopsin (see inset of Figure 9) strongly suggests that the excess of octyl glucoside is lost in the subphase and that rhodopsin surface concentration increases accordingly. Therefore, the surface pressure decrease observed after monolayer spreading or during compression is very likely due to the loss of octyl glucoside in the subphase, which results in rhodopsin unfolding (Figures 3 and 5).

Conditions that Retain the Secondary Structure of Rhodopsin and Its Organization in Monolayers. The spectra shown in Figures 6, 8, and 9 are very similar to the one of ROS membranes in solution (Figure 2). These data thus suggest that it is possible to retain the secondary structure of rhodopsin when the film is maintained at a surface pressure of at least 4.5 mN m^{-1} (Figure 6) or when measurements

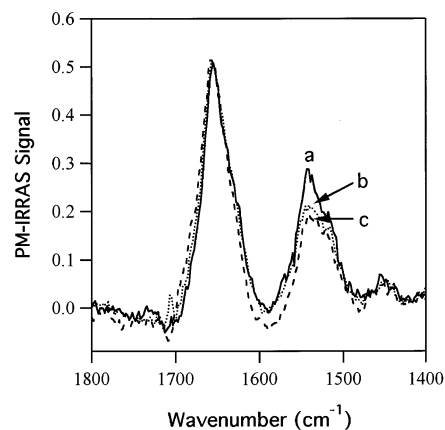


FIGURE 11: Normalized PM-IRRAS spectra of rhodopsin at 20 mN m^{-1} using the amide I band. Spectrum a (solid line) is the spectrum at 120 min in Figure 9 (this spectrum is identical to the one at 0 min; see inset of Figure 9), whereas spectra b (dotted line) and c (broken line) are the spectra at 20 mN m^{-1} in Figures 6 and 8, respectively. Spectra were normalized using the amide I band.

are performed at $4 \text{ }^\circ\text{C}$ (Figures 8 and 9). Moreover, the good agreement between the thickness value of rhodopsin measured under conditions allowing to retain its secondary structure (Figure 7) compared to the value determined from its crystal structure (38, 39) also supports this conclusion. Such conditions could eventually be used in an attempt to prepare two-dimensional crystals of rhodopsin. It thus is important to determine if the secondary structure and the orientation of rhodopsin at 20 mN m^{-1} were similar when spreading is performed at 5 or 10 mN m^{-1} and compressed immediately at 4 and $21 \text{ }^\circ\text{C}$, respectively, or when the film is maintained at 20 mN m^{-1} for 120 min at $4 \text{ }^\circ\text{C}$. Figure 11 shows the normalized PM-IRRAS spectra of rhodopsin at 20 mN m^{-1} extracted from Figure 9 (spectrum after 120 min incubation; spectrum a, Figure 11), Figure 6 (spectrum b, Figure 11), and Figure 8 (spectrum c, Figure 11). It can be seen that the shape of the amide I band of all spectra is almost identical, which suggests that the structure of rhodopsin remains unchanged regardless of the experimental condition. Moreover, the AI/AII ratio of the spectrum after 120 min incubation is slightly different when compared to the spectra when spreading is performed at 5 ($4 \text{ }^\circ\text{C}$) or 10 mN m^{-1} ($21 \text{ }^\circ\text{C}$). Given that the spectra after 0 and 120 min are identical (see inset of Figure 8) and that the experimental conditions used for the measurement of the spectra in Figures 8 and 9 are the same, the AI/AII ratio of these spectra should have been very similar. Nevertheless, the small difference between these AI/AII ratios suggest that the orientation of the α -helices of rhodopsin under these different experimental conditions is only slightly different.

Effect of Surface Pressure on the Secondary Structure and the Orientation of Rhodopsin. PM-IRRAS signal increases with surface pressure, suggesting an increase in rhodopsin surface concentration. This change can also be attributed to structural or orientational changes upon compression to higher surface pressures. The amide I/amide II ratio (AI/AII) was used to estimate the relative orientation change taking place during compression. Indeed, it was previously reported (43) that the AI/AII ratio can vary from -1 to 6.5 when individual α -helices are oriented, respectively, parallel and perpendicular to the normal to the interface. To visualize those changes, if any, we compared normalized spectra of

rhodopsin monolayers at 10 and 30 mN m⁻¹ (see inset of Figures 6 and 8). It can be seen that the shape of the amide I band of rhodopsin is very similar at both surface pressures whereas the AI/AII ratio slightly decreases with surface pressure. Indeed, a ratio of 3.3 and 2.5 is obtained at 10 and 30 mN m⁻¹, respectively. It is thus clear from these spectra that compression to higher surface pressures did not affect the secondary structure of rhodopsin. However, the orientation of the α -helices of rhodopsin slightly changes when increasing the surface pressure, although this change cannot be attributed to any individual α -helix of rhodopsin. Indeed, the slight decrease of the AI/AII ratio suggests that the α -helices of purified rhodopsin become slightly closer to each other and more parallel to the normal upon compression.

Organization of ROS Disk Membranes in Monolayers. Several differences can be observed when the PM-IRRAS spectra of ROS disk membranes in monolayers (Figure 10) are compared with the PM-IRRAS spectra of rhodopsin under conditions where unfolding is prevented (Figures 6 and 8) as well as with the spectrum of ROS disk membranes in solution (Figure 2). In Figure 10, the intensity of the ester carbonyl band at 1740 cm⁻¹ is much stronger than that of the amide I band, whereas it is a much weaker band in Figure 2. This difference can be explained by the selection rules in PM-IRRAS. Indeed, it has been determined (71) that an upward-oriented band indicates a transition moment occurring preferentially in the plane of the monolayer, whereas a downward-oriented band reveals an orientation preferentially perpendicular to the monolayer. For a given oscillator strength, bands associated with transition moments that are parallel to the surface are more intense than those perpendicular to the surface (43). Such a large intensity of the band at 1740 cm⁻¹ could be explained if the ester carbonyl group of the ROS membrane phospholipids were oriented parallel to the surface as previously demonstrated for pure phospholipids (43). Moreover, the ROS membrane phospholipids might partly remain as bilayers upon spreading, and such a phenomenon could thus contribute to the larger intensity of the ester carbonyl band compared to the amide I band observed in Figure 10. The data of Korenbrot and Pramik (8) and Salesse et al. (4) support this possibility. Indeed, Korenbrot and Pramik (8) have shown by electron microscopy that rhodopsin-egg phosphatidylcholine monolayer films transferred onto glass consisted of nonoverlapping, randomly distributed membrane fragments separated by a lipid monolayer. Salesse et al. (4) observed that ROS disk membranes spread in monolayers form multilayers at collapse pressure and that this property is facilitated by the presence of a shell of phospholipids surrounding rhodopsin in these films. Moreover, the difference in the intensity of the amide I band of pure rhodopsin monolayers compared to that of ROS disk membranes at the same surface pressure (compare Figures 6 and 8 with Figure 10) can be partly explained by the decrease in rhodopsin surface concentration due to the presence of the ROS disk membrane phospholipids. Rhodopsin is thus more diluted in ROS disk membranes than when it is spread as a pure component. There are 72 phospholipids per rhodopsin (69), and ROS membrane phospholipids have an average molecular area of 0.67 nm² molecule⁻¹ at 24 mN m⁻¹ (72). By assuming that ROS disk membranes retain their bilayer organization in monolayers, these phospholipids will occupy an area of \sim 24 nm² per molecule of rhodopsin. Thus,

a total area of 37.1 nm² molecule⁻¹ can be calculated for rhodopsin in ROS disk membranes when taking into account the area of pure rhodopsin (13.1 nm² molecule⁻¹) (38, 39) and its surrounding phospholipids (24.0 nm² molecule⁻¹). Rhodopsin thus accounts for only \sim 33% of this area. These data can thus at least partly explain the reduced intensity of the amide I band in the spectra of Figure 10 compared to those shown in Figures 6 and 8 as well as the large intensity of the ester carbonyl band at 1740 cm⁻¹ compared to that of the amide I band (Figure 10) since ROS disks membrane phospholipids account for \sim 66% of the area in these films.

The position of the amide I band at approximately 1655 cm⁻¹ suggests that the presence of lipids surrounding rhodopsin prevent its unfolding in monolayers even when spreading is performed at 0 mN m⁻¹. This is particularly important in view of the sensitivity of pure rhodopsin to the spreading surface pressure. Moreover, the AI/AII ratio in these films is close to 1, which contrasts with the ratios of 2.5–3.3 observed for pure rhodopsin (compare Figure 10 with Figures 6 and 8). The AI/AII ratio can vary from -1 to 6.5 when individual α -helices are oriented, respectively, parallel and perpendicular to the normal to the interface (43). In contrast, rhodopsin contains 7 α -helices linked together by loops which cannot act as individual, independent α -helices. The ratio obtained for purified rhodopsin and for ROS disk membranes must thus be compared with care. The large change in the AI/AII ratio observed in Figure 10 compared to Figures 6 and 8 cannot be attributed to any individual α -helix of rhodopsin. However, it can be postulated that the large difference between the AI/AII ratio of rhodopsin and ROS disk membranes suggests that the α -helices of rhodopsin in ROS disk membranes are closer to each other and more parallel to the normal than when purified rhodopsin is spread in monolayers. This suggests that the orientation of the α -helices of rhodopsin in monolayers is very different when it is surrounded by detergent compared to when it is surrounded by ROS disk membrane phospholipids.

CONCLUSION

This paper thus shows evidence that experimental conditions can be found where the secondary structure of membrane proteins such as rhodopsin can be retained when spread in monolayers. The present data demonstrate that *in situ* infrared spectroscopy can provide direct information on the secondary structure of proteins in such films. Finally, it must keep in mind that, although we have determined the conditions that retain the secondary structure of rhodopsin in monolayers which are also likely valid for other G-protein coupled receptors, the present conditions may not work for other types of membrane proteins, and the secondary structure of each individual protein must be assessed prior to drawing conclusions on their properties when spread in monolayers. Moreover, the data obtained with ROS disk membranes suggest that spreading membranes in monolayers represent an appropriate model to study the interaction of membrane proteins with other proteins such as G-proteins.

REFERENCES

1. Dynarowicz-Latka, P., Dhanabalan, A., and Oliveira, O. N. (2001) Modern physicochemical research on Langmuir monolayers, *Adv. Colloid Interface Sci.* 91, 221–294.

2. Kaganer, V. M., Mohwald, H., and Dutta, P. (1999) Structure and phase transitions in Langmuir monolayers, *Rev. Mod. Phys.* **71**, 779–820.
3. Vollhardt, D., and Fainerman, V. B. (2000) Penetration of dissolved amphiphiles into two-dimensional aggregating lipid monolayers, *Adv. Colloid Interface Sci.* **86**, 103.
4. Salesse, C., Ducharme, D., Leblanc, R. M., and Boucher, F. (1990) Estimation of disk membrane lateral pressure and molecular area of rhodopsin by the measurement of its orientation at the nitrogen-water interface from an ellipsometric study, *Biochemistry*. **29**, 4567–4575.
5. Pepe, I. M., Maxia, L., and Nicolini, C. (1996) Properties of Langmuir–Blodgett films of rhodopsin, *Thin Solid Films* **284–285**, 739–742.
6. Maxia, L., Radicchi, G., Pepe, I. M., and Nicolini, C. (1995) Characterization of Langmuir–Blodgett films of rhodopsin: thermal stability studies, *Biophys. J.* **69**, 1440–1446.
7. Korenbrot, J. I., and Jones, O. (1979) Linear dichroism of rhodopsin in air–water interface films, *J. Membr. Biol.* **46**, 239–254.
8. Korenbrot, J. I., and Pramik, M. J. (1977) Formation, structure, and spectrophotometry of air–water interface films containing rhodopsin, *J. Membr. Biol.* **37**, 235–262.
9. Karan, H. I., Hirsch, R. E., and Brody, S. S. (1978) Stability and regeneration of rhodopsin absorption spectra at an air–water interface. *Z Naturforsch. C* **33**, 317–320.
10. Alegria, G., and Dutton, P. L. (1991) Langmuir–Blodgett monolayer films of bacterial photosynthetic membranes and isolated reaction centers: preparation, spectrophotometric and electrochemical characterization, *Biochim. Biophys. Acta* **1057**, 239–257.
11. Fang, J. Y., Gaul, D. F., Chumanov, G., and Cotton, T. M. (1995) Characterization of photosynthetic reaction centers from *Rhodospira rubra* at the air–water interface and in Langmuir–Blodgett films, *Langmuir* **11**, 4366–4370.
12. Hirata, Y., Nukanobu, K., Hara, M., Asada, Y., Miyake, J., and Fujihira, M. (1992) Preparation of stable Langmuir–Blodgett films of photosynthetic bacterial reaction center from *Rhodospseudomonas viridis* using poly-L-lysine, *Chem. Lett.* **12**, 2277–2280.
13. Uphaus, R. A., Fang, J. Y., Picorel, R., Chumanov, G., Wang, J. Y., Cotton, T. M., and Seibert, M. (1997) Langmuir–Blodgett and X-ray diffraction studies of isolated photosystem II reaction centers in monolayers and multilayers: physical dimensions of the complex, *Photochem. Photobiol.* **65**, 673–679.
14. Gallant, J., Desbat, B., Vaknin, D., and Salesse, C. (1998) Polarization-modulated infrared spectroscopy and X-ray reflectivity of photosystem II core complex at the gas–water interface, *Biophys. J.* **75**, 2888–2899.
15. Gallant, J., Lavoie, H., Tessier, A., Munger, G., Leblanc, R. M., and Salesse, C. (1998) Surface and spectroscopic properties of photosystem II core complex at the nitrogen/water interface, *Langmuir* **14**, 3954–3963.
16. Faivre, V., Manivet, P., Callaway, J. C., Airaksinen, M. M., Morimoto, H., Baszkin, A., Launay, J. M., and Rosilio, V. (2000) Ligand interaction with the purified serotonin transporter in solution and at the air/water interface, *FEBS Lett.* **471**, 56–60.
17. Faivre, V., Rosilio, V., Manivet, P., Langevin, D., Launay, J. M., and Baszkin, A. (2001) Molecular organization of the human serotonin transporter at the air/water interface, *FEBS Lett.* **492**, 14–19.
18. Pattus, F., Desnuelle, P., and Verger, R. (1978) Spreading of liposomes at the air/water interface, *Biochim. Biophys. Acta* **507**, 62–70.
19. Schurholz, T., and Schindler, H. (1991) Lipid–protein surface films generated from membrane vesicles: self-assembly, composition, and film structure, *Eur. Biophys. J.* **20**, 71–78.
20. Karan, H. I., and Brody, S. S. (1975) Studies on fragments of rod outer segments from bovine retinas, *Z Naturforsch. C* **30**, 796–799.
21. Azuma, K., and Takagi, M. (1966) in *Annual Report of Biological Works* pp 1473–1481, Osaka University, Osaka.
22. Korenbrot, J. I., and Hwang, S. B. (1980) Proton transport by bacteriorhodopsin in planar membranes assembled from air–water interface films, *J. Gen. Physiol.* **76**, 649–682.
23. Méthot, M., Boucher, F., Salesse, C., Subirade, M., and Pézolet, M. (1996) Determination of bacteriorhodopsin orientation in monolayers by infrared spectroscopy, *Thin Solid Films*. **284–285**, 627–630.
24. Min, J., Choi, H. G., Oh, B. K., Lee, W. H., Paek, S. H., and Choi, J. W. (2001) Visual information processing using bacteriorhodopsin-based complex LB films, *Biosens. Bioelectron.* **16**, 917–923.
25. Verclas, S. A., Howes, P. B., Kjaer, K., Wurlitzer, A., Weygand, M., Buldt, G., Dencher, N. A., and Losche, M. (1999) X-ray diffraction from a single layer of purple membrane at the air/water interface, *J. Mol. Biol.* **287**, 837–843.
26. Volkov, V., Svirko, Y. P., Kamalov, V. F., Song, L., and El-Sayed, M. A. (1997) Optical rotation of the second harmonic radiation from retinal in bacteriorhodopsin monomers in Langmuir–Blodgett film: evidence for nonplanar retinal structure, *Biophys. J.* **73**, 3164–3170.
27. Hwang, S. B., Korenbrot, J. I., and Stoekenius, W. (1977) Proton transport by bacteriorhodopsin through an interface film, *J. Membr. Biol.* **36**, 137–158.
28. Hwang, S. B., Korenbrot, J. I., and Stoekenius, W. (1977) Structural and spectroscopic characteristics of bacteriorhodopsin in air–water interface films, *J. Membr. Biol.* **36**, 115–135.
29. Blaudez, D., Boucher, F., Buffeteau, T., Desbat, B., Grandbois, M., and Salesse, C. (1999) Anisotropic optical constants of bacteriorhodopsin in the mid-infrared: consequence on the determination of α -helix orientation, *Appl. Spectrosc.* **53**, 1299–1304.
30. Pattus, F., Rothen, C., Streit, M., and Zahler, P. (1981) Further studies on the spreading of biomembranes at the air/water interface: Structure, composition, enzymatic activities of human erythrocyte and sarcoplasmic reticulum membrane films, *Biochim. Biophys. Acta* **647**, 29–39.
31. Kanno, T., Setaka, M., Hongo, T., and Kwan, T. (1983) Spontaneous formation of a monolayer membrane from sarcoplasmic reticulum at an air–water interface. *J. Biochem. (Tokyo)* **94**, 473–477.
32. Pattus, F., Piovant, M. C., Lazdunski, C. J., Desnuelle, P., and Verger, R. (1978) Spreading of biomembranes at the air/water interface, *Biochim. Biophys. Acta* **507**, 71–82.
33. Oliveira, R. G., Calderon, R. O., and Maggio, B. (1998) Surface behavior of myelin monolayers, *Biochim. Biophys. Acta* **1370**, 127–137.
34. Calderon, R. O., Maggio, B., Neuberger, T. J., and De Vries, G. H. (1993) Surface behavior of axolemma monolayers: physicochemical characterization and use as supported planar membranes for cultured Schwann cells, *J. Neurosci. Res.* **34**, 206–218.
35. Calderon, R. O., Maggio, B., Neuberger, T. J., and DeVries, G. H. (1995) Modulation of Schwann cell Po glycoprotein and galactocerebroside by the surface organization of axolemma, *J. Neurosci. Res.* **40**, 349–358.
36. MacRitchie, F. (1986) Spread monolayers of proteins, *Adv. Colloid Interface Sci.* **25**, 341–385.
37. Amis, E. J., Davenport, D. A., and Yu, H. (1981) Photopigment content of isolated bovine disk membrane vesicles, *Anal. Biochem.* **114**, 85–91.
38. Teller, D. C., Okada, T., Behnke, C. A., Palczewski, K., and Stenkamp, R. E. (2001) Advances in determination of a high-resolution three-dimensional structure of rhodopsin, a model of G-protein-coupled receptors (GPCRs), *Biochemistry* **40**, 7761–7772.
39. Palczewski, K., Kumasaka, T., Hori, T., Behnke, C. A., Motoshima, H., Fox, B. A., Le Trong, I., Teller, D. C., Okada, T., Stenkamp, R. E., Yamamoto, M., and Miyano, M. (2000) Crystal structure of rhodopsin: A G protein-coupled receptor, *Science* **289**, 739–745.
40. Als-Nielsen, J., and Kjaer, K. (1989) Phase transitions in soft condensed matter, *Proc. NATO Adv. Stud. Inst.* **211**, 113–138.
41. Dluhy, R., and Mendelsohn, R. (1988) Emerging techniques in biophysical FT-IR, *Anal. Chem.* **60**, 269A–278A.
42. Blaudez, D., Buffeteau, T., Cornut, J. C., Desbat, B., Escafre, N., Pézolet, M., and Turlet, J. M. (1993) Polarization-modulated FT-IR spectroscopy of a spread monolayer at the air–water interface, *Appl. Spectrosc.* **47**, 869–874.
43. Cornut, I., Desbat, B., Turlet, J. M., and Dufourcq, J. (1996) In situ study by polarization modulated Fourier transform infrared spectroscopy of the structure and orientation of lipids and amphipathic peptides at the air–water interface, *Biophys. J.* **70**, 305–312.
44. Castano, S., Desbat, B., Laguerre, M., and Dufourcq, J. (1999) Structure, orientation and affinity for interfaces and lipids of ideally amphipathic lytic LiKj(i=2j) peptides, *Biochim. Biophys. Acta* **1416**, 176–194.

45. Castano, S., Desbat, B., and Dufourcq, J. (2000) Ideally amphipathic beta-sheeted peptides at interfaces: structure, orientation, affinities for lipids and hemolytic activity of (KL)(m)K peptides, *Biochim. Biophys. Acta* 1463, 65–80.
46. Ulrich, W. P., and Vogel, H. (1999) Polarization-modulated FTIR spectroscopy of lipid/gramicidin monolayers at the air/water interface, *Biophys. J.* 76, 1639–1647.
47. Dluhy, R. A., Reilly, K. E., Hunt, R. D., Mitchell, M. L., Mautone, A. J., and Mendelsohn, R. (1989) Infrared spectroscopic investigations of pulmonary surfactant. Surface film transitions at the air–water interface and bulk phase thermotropism, *Biophys. J.* 56, 1173–1181.
48. Flach, C. R., Brauner, J. W., Taylor, J. W., Baldwin, R. C., and Mendelsohn, R. (1994) External reflection FTIR of peptide monolayer films in situ at the air/water interface: experimental design, spectra-structure correlations, and effects of hydrogen–deuterium exchange, *Biophys. J.* 67, 402–410.
49. Flach, C. R., Prendergast, F. G., and Mendelsohn, R. (1996) Infrared reflection–absorption of melittin interaction with phospholipid monolayers at the air/water interface, *Biophys. J.* 70, 539–546.
50. Wu, F., Flach, C., Seaton, B., Mealy, T., and Mendelsohn, R. (1999) Stability of annexin V in ternary complexes with Ca²⁺ and anionic phospholipids: IR studies of monolayer and bulk phases, *Biochemistry* 38, 792–799.
51. Dieudonne, D., Mendelsohn, R., Farid, R. S., and Flach, C. R. (2001) Secondary structure in lung surfactant SP-B peptides: IR and CD studies of bulk and monolayer phases, *Biochim. Biophys. Acta* 1511, 99–112.
52. Salesse, C., Boucher, F., and Leblanc, R. M. (1984) An evaluation of purity criteria for bovine rod outer segment membranes, *Anal. Biochem.* 142, 258–266.
53. Smith, H. G., Jr., and Litman, B. J. (1982) Preparation of osmotically intact rod outer segment disks by Ficoll flotation, *Methods Enzymol.* 81, 57–61.
54. Salesse, C., Leblanc, R. M., and Kito, Y. (1988) Lipid contamination of disks depends on rod outer-segment purity, *Exp. Eye Res.* 46, 285–287.
55. Litman, B. J. (1982) Purification of rhodopsin by concanavalin A affinity chromatography, *Methods Enzymol.* 81, 150–153.
56. Trurnit, H. J. (1960) A theory and method for the spreading of protein monolayers, *J. Colloid Sci.* 15, 1–13.
57. Blaudez, D., Turlet, J.-M., Dufourcq, J., Bard, D., Buffeteau, T., and Desbat, B. (1996) Investigation at the air/water interface using polarization modulation IR spectroscopy, *J. Chem. Soc., Faraday Trans.* 92, 525–530.
58. Als-Nielsen, J., and Pershan, P. S. (1983) Synchrotron x-ray diffraction study of liquid surface, *Nucl. Instrum. Meth.* 208, 545–548.
59. Vaknin, D. (2001) in *Methods in Materials Research* (Kaufmann, E. N., Ed.) pp 10d.2.1–10.d.2.21, John Wiley & Sons, New York.
60. Parratt, L. G. (1954) Surface studies of solids by total reflection of x-rays, *Phys. Rev.* 59, 359–369.
61. Ocko, B. M., Wu, X. Z., Sirota, E. B., Sinha, S. K., and Deutsch, M. (1994) X-ray reflectivity study of thermal capillary waves on liquid surfaces, *Phys. Rev. Lett.* 72, 242–245.
62. Tiede, D. M. (1985) Incorporation of membrane proteins into interfacial films: model membranes for electrical and structural characterization, *Biochim. Biophys. Acta* 811, 357–379.
63. Pistorius, A. M., and de Grip, W. J. (1994) Rhodopsin's secondary structure revisited: assignment of structural elements, *Biochem. Biophys. Res. Commun.* 198, 1040–1045.
64. Rothschild, K. J., DeGrip, W. J., and Sanches, R. (1980) Fourier transform infrared study of photoreceptor membrane. I. Group assignments based on rhodopsin delipidation and reconstitution, *Biochim. Biophys. Acta* 596, 338–351.
65. Miljanich, G. P., Nemes, P. P., White, D. L., and Dratz, E. A. (1981) The asymmetric transmembrane distribution of phosphatidylethanolamine, phosphatidylserine, and fatty acids of the bovine retinal rod outer segment disk membrane, *J. Membr. Biol.* 60, 249–255.
66. Krimm, S., and Bandekar, J. (1986) Vibrational spectroscopy and conformation of peptides, polypeptides, and proteins, *Adv. Protein. Chem.* 38, 181–364.
67. Dousseau, F., and Pézolet, M. (1990) Determination of the secondary structure content of proteins in aqueous solutions from their amide I and amide II infrared bands. Comparison between classical and partial least-squares methods, *Biochemistry* 29, 8771–8779.
68. Arrondo, J. L., Muga, A., Castresana, J., and Goni, F. M. (1993) Quantitative studies of the structure of proteins in solution by Fourier transform infrared spectroscopy, *Prog. Biophys. Mol. Biol.* 59, 23–56.
69. Goormaghtigh, E., Cabiaux, V., and Ruyschaert, J. M. (1994) Determination of soluble and membrane protein structure by Fourier transform infrared spectroscopy. I. Assignments and model compounds, *Subcell. Biochem.* 23, 329–362.
70. Surewicz, W. K., Mantsch, H. H., and Chapman, D. (1993) Determination of protein secondary structure by Fourier transform infrared spectroscopy: a critical assessment, *Biochemistry* 32, 389–394.
71. Blaudez, D., Buffeteau, T., Cornut, J. C., Desbat, B., Escafre, N., Pézolet, M., and Turlet, J. M. (1994) Polarization modulation FTIR spectroscopy at the air–water interface, *Thin Solid Films* 242, 146–150.
72. Ducharme, D., Salesse, C., and Leblanc, R. M. (1985) Ellipsometric studies of rod outer segment phospholipids at the nitrogen–water interface, *Thin Solid Films* 132, 83–90.

BI026004T